Theoretical Study of Doubly Resonant Sum-Frequency Vibrational Spectroscopy for 1,1′-Bi-2-naphthol Molecules on Water Surface

ARTICLE *in* THE JOURNAL OF PHYSICAL CHEMISTRY C · MAY 2013

Impact Factor: 4.77 · DOI: 10.1021/jp400818d

5 AUTHORS, INCLUDING:

Renhui Zheng
Chinese Academy of Sciences
55 PUBLICATIONS **445** CITATIONS
SEE PROFILE

Qiang Shi
Chinese Academy of Sciences
101 PUBLICATIONS **2,410** CITATIONS
SEE PROFILE

THE JOURNAL OF PHYSICAL CHEMISTRY C

Article

pubs.acs.org/JPCC

Theoretical Study of Doubly Resonant Sum-Frequency Vibrational Spectroscopy for 1,1′-Bi-2-naphthol Molecules on Water Surface

Ren-hui Zheng,*[,†] Wen-mei Wei,[‡] Yuan-yuan Jing,[†] Hao Liu,[†] and Qiang Shi*[,†]

[†]Beijing National Laboratory for Molecular Sciences, State Key Laboratory for Structural Chemistry of Unstable and Stable Species, Institute of Chemistry, Chinese Academy of Sciences, Zhongguancun, Beijing 100190, People's Republic of China

[‡]Department of Chemistry, College of Basic Medicine, Anhui Medical University, Hefei, Anhui 230032, People's Republic of China

Supporting Information

ABSTRACT: By combining molecular dynamics (MD) simulation and density functional theory (DFT) calculations, we investigate the surface doubly resonant sum-frequency vibrational spectroscopy (SFVS) for a monolayer of R-1,1′-bi-2-naphthol (R-BN) molecules on water surface. MD simulations indicate that the R-BN molecules stand perpendicularly on the water surface due to hydrogen bonding with the water molecules. DFT and time-dependent density functional theory (TDDFT) methods are employed to obtain potential energy shifts, transition dipoles, and their derivatives, which are then used to calculate both the Franck−Condon and Herzberg−Teller terms to the surface hyperpolarizabilities. The theoretical SFVS agrees well with the experimental result. The origin of the SFVS peaks and symmetry properties of the hyperpolarizabilities tensor are also analyzed, which indicates that theoretical computations can obtain the most important components that are helpful for experimental SFVS analysis. The current work shows that theoretical calculations can provide useful detailed molecular information, such as molecular structure, orientation, and excited structure at interfaces, in studies of surface doubly resonant SFVS.

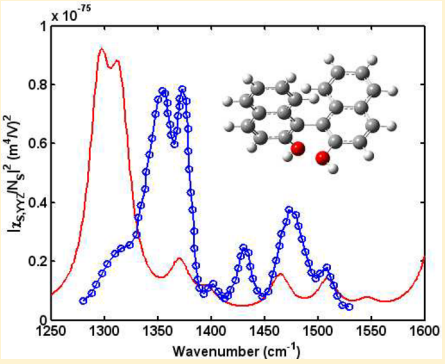

1. INTRODUCTION

In recent years, surface sum-frequency vibrational spectroscopy (SFVS) has developed into an important tool to study molecular orientation, structure, and dynamics at interfaces.[1−9] Depending on whether the UV/visible frequency is in resonance with the electronic transition of the molecule, SFVS can be classified into three types: doubly resonant IR-UV SFVS,[10] SFVS off electronic resonance,[11] and sum-frequency generation near electronic resonance.[12,13]

Most surface SFVS studies are off electronic resonance. Recently, Raschke et al. performed experimental studies of doubly resonant infrared-visible sum-frequency for adsorbed monolayers of Rhodamine 6G on fused quartz.[14] Belkin and Shen[10] detected the vibrational spectra of a monolayer of R-1,1′-bi-2-naphthol (R-BN) on water due to strong resonant enhancement using surface doubly resonant IR-UV SFVS. Chen et al.[15] applied SFVS to investigate the cell membrane and its interaction with membrane-active molecules. These studies have found that doubly resonant IR-UV SFVS can significantly improve sensitivity by 2 or 3 orders of magnitude.[10,14,15] In addition, the doubly resonant SFVS has also been found to be able to study the molecular excited structure at interfaces.[10,14]

Both surface doubly resonant IR-UV SFVS and SFVS off electronic resonance are capable of determining the molecule orientation at interfaces, but their molecular origins are different: SFVS off electronic resonance is related to the nonresonant Raman polarizability, while doubly resonant IR-UV SFVS is related to the resonant Raman polarizability. Theoretically, two different terms are considered in calculating the Raman polarizability:[16] Raman A term originates from the Franck−Condon progression that depends on the displacements of potential energy surfaces between the ground and excited electronic states, the electric transition dipole moments, and the line width of the resonant excited state; Raman B term is a Herzberg−Teller term that depends on the electric transition dipole moments and their derivatives. Both Raman A and B terms contribute to resonant Raman while only Raman B term contributes to nonresonant Raman. As a result, resonant and nonresonant SFVS can be rather different. For example, in a resonant case, for a totally symmetric vibrational mode, the Raman A term is generally much larger than the Raman B term and dominates the Raman polarizability; for a non-totally symmetric vibrational mode, the Raman A term is zero if the symmetry is not changed upon excitation and only Raman B term contributes to Raman polarizability.[16] Doubly resonant SFVS are calculated using the sum-over-states method. Only the resonant excited states are included to simplify the calculation, and both the Raman A and B terms are taken into consideration. In principle, SFVS off electronic resonance can also be calculated using the sum-over-states method. However, in this case, the summation needs to include many

Received: January 24, 2013
Revised: April 28, 2013
Published: May 8, 2013

dx.doi.org/10.1021/jp400818d | J. Phys. Chem. C 2013, 117, 11117−11123

high-lying excited states, and it is hard technically to obtain the accurate transition energies and dipole transition moment derivatives for the highly excited states using current quantum chemistry calculations. Thus, the SFVS off electronic resonance and nonresonant Raman are more often computed using the frequency-independent or frequency-dependent polarizability from the ground state calculations.[17−25]

Due to the resonant enhancement, the intensity of resonant Raman is much larger than nonresonant Raman by 2 or 3 orders of magnitude.[16] This is also the reason why the intensity of doubly resonant IR-UV SFVS can be significantly enhanced. Thus, doubly resonant IR-UV SFVS is more sensitive and can be applied to detect low-concentration matter at interfaces.

Theoretically, the molecular structure and vibrational frequencies, and the frequency-dependent nonresonant Raman transition polarizabilities can all be obtained through the ground state calculations when we study SFVS off electronic resonance. However, in order to investigate the doubly resonant IR-UV SFVS, apart from calculating the ground state properties, excited state properties such as electric transition dipole moments, and the displacements between the excited and ground states are also necessary. It is known that there are 27 components of the hyperpolarizability and scientists can only obtain four independent surface susceptibilities by experiment. It is hard to get all the components of hyperpolarizability from experiment if the molecule has no symmetry. On the other hand, quantum calculations can get all the components of the hyperpolarizability and identify the most important components, which are helpful for SFVS experimental analysis.

Though there are several theoretical studies[17−25] on surface SFVS off electronic resonance, which studied the molecule distribution, orientation, and interactions at interfaces, few theoretical investigations have been performed on surface doubly resonant IR-UV SFVS. Especially, to the best of our knowledge, no ab initio calculation of doubly resonant surface hyperpolarizability was performed in the literature. In this paper, by applying the molecular dynamics (MD) simulations, we study the molecular structure and orientation of R-BN on water surface, and then by using quantum chemical computations, the resonant Raman polarizabilities and the corresponding doubly resonant hyperpolarizabilities are obtained. Finally, by combining the MD simulations and ab initio studies, we are able to obtain the surface SFVS for R-BN and compare theoretical results with the experimental ones.

2. THEORY

In the electric-dipole approximation, the surface SFVS signal at $\omega = \omega_1 + \omega_2$ is given by[10,14]

$$S(\omega) \propto |\chi_S^{(2)}|^2 I_1(\omega_1) I_2(\omega_2) \tag{1}$$

where I_i (ω_i) is the intensity of the light wave at frequency ω_i. $\chi_S^{(2)}$ is the surface nonlinear susceptibility, which can be written in terms of the second-order molecular hyperpolarizability $\alpha^{(2)}$

$$\chi_S^{(2)} = \frac{N_S L_S}{\varepsilon_0} \langle \alpha^{(2)} \rangle \tag{2}$$

where N_S is the surface molecular density, L_S is the local correction factor, ε_0 is the dielectric constant, and the angular brackets denote the orientational average. In ref 26, Moad and Simpson presented a derivation of the relationships between macroscopic and molecular hyperpolarizabilities. The molecular and laboratory coordinate systems are related through three Euler angles θ (tilt angle), ψ (twist angle), and ϕ (in-plane rotation angle). For a film with a random orientation distribution within the surface plane, the in-plane rotation angle is isotropic and there are four elements in the $\chi_S^{(2)}$ tensors for SFVS in uniaxial systems, which are $\chi_{S,ZZZ}$, $\chi_{S,ZXX} = \chi_{S,ZYY}$, $\chi_{S,XZX} = \chi_{S,YZY}$, $\chi_{S,XXZ} = \chi_{S,YYZ}$. The detailed expressions are not presented here for simplicity. From these expressions we can know that no SFVS can be observed if the distributions of the three Euler angles are isotropic. This property of $\chi_S^{(2)}$ plays an important role in the surface-sensitivity of the SFVS.

In the doubly resonant case, the SFVS molecular hyperpolarizability can be written into[10]

$$\alpha^{(2)}_{\sigma\rho\kappa}(\nu, \nu_2) = \frac{1}{h^2} \frac{\langle Gg'|\mu_\kappa|Gg\rangle}{(\nu_2 - \nu_{Gg',Gg} + i\Gamma_{gg'})} \times \sum_{M,m} \left[\frac{\langle Gg|\mu_\sigma|Mm\rangle\langle Mm|\mu_\rho|Gg'\rangle}{(\nu - \nu_{Mm,Gg} + i\Gamma_{Mm})} \right] \tag{3}$$

where G and M represent ground and excited electronic states, respectively, while g, g', and m represent vibrational levels. μ_σ, μ_ρ, and μ_κ are the dipole moment operators, $\nu_{Mm,Gg}$ and $\nu_{Gg',Gg}$ are the frequency differences between the indicated vibronic levels, Γ_{Mm} is the damping parameter of the Mth electronic state and $\Gamma_{gg'}$ is the line width of the ground state.

Equation 3 can be rewritten into

$$\alpha^{(2)}_{\sigma\rho\kappa}(\nu, \nu_2) = \frac{1}{h} \sqrt{\frac{h}{8\pi^2 \nu_t}} \frac{\partial\langle G|\mu_\kappa|G\rangle}{\partial Q_t} \times \frac{1}{(\nu_t - \nu_2 - i\Gamma_{gg'})} \alpha_{\sigma\rho} \tag{4}$$

where ν_t is the vibrational frequency of the t mode and Q_t is the normal coordinate, and anti-Stoke resonant Raman polarizability $\alpha_{\sigma\rho}$ is given by a Taylor expansion of the transition moments in terms of the molecular normal modes[27−29]

$$\alpha_{\sigma\rho} = A_{\sigma\rho} + B_{\sigma\rho} \tag{5}$$

where

$$A_{\sigma\rho} = \sum_M \Delta_t \exp(-\Delta_t^2) \times \frac{\langle G|\mu_\sigma|M\rangle_0\langle M|\mu_\rho|G\rangle_0}{h} \times \left\{ \frac{1}{\Delta\nu_0 - i\Gamma_M} - \frac{1}{\Delta\nu_0 + \nu_t - i\Gamma_M} \right\} \tag{6}$$

$$B_{\sigma\rho} = \frac{1}{h} \sum_M \sqrt{\frac{h}{8\pi^2\nu_t}} \exp(-\Delta_t^2) \left[\frac{1}{\Delta\nu_0 - i\Gamma_M} \{(1 - \Delta_t^2)\langle G| \mu_\sigma|M\rangle_0 (\partial\langle M|\mu_\rho|G\rangle/\partial Q_t)_0 - \Delta_t^2 (\partial\langle G|\mu_\sigma|M\rangle/\partial Q_t)_0 \langle M|\mu_\rho|G\rangle_0\} + \frac{1}{\Delta\nu_0 + \nu_t - i\Gamma_M} \{(\partial\langle G|\mu_\sigma|M\rangle/\partial Q_t)_0 \langle M|\mu_\rho|G\rangle_0 + \Delta_t^2 \langle G|\mu_\sigma|M\rangle_0 (\partial\langle M|\mu_\rho|G\rangle/\partial Q_t)_0\} \right] \tag{7}$$

In eqs 6 and 7, Δ_t is the displacement of potential energy minimum along the normal coordinate Q_t between the ground and excited states, and $\Delta\nu_0 = \nu_{MG} - \nu$. In resonant Raman and surface doubly resonant SFVS, generally Raman A term dominants, thus, Raman and SFVS intensity is proportional to the square of the displacements when only the Raman A term is considered. Equation 7 shows that the Raman B term is also independent of the signs of the displacements. We know

dx.doi.org/10.1021/jp400818d | J. Phys. Chem. C 2013, 117, 11117−11123

that the bulk doubly resonant SFVS is from the Raman B term.[10] However, if both Raman A and B terms are taken into consideration in surface doubly resonant SFVS, the signs of the displacements may affect the result. So the surface doubly resonant and near resonant SFVS may be sensitive to the signs of displacements, when the magnitude of Raman A and B term are comparable depending on the displacements and UV detuning. Theoretically, the signs of the displacements can be obtained from quantum chemical computations directly.

3. RESULTS AND DISCUSSION

3.1. Molecular Dynamics Simulations. The molecular structure of R-BN and the Euler angles relating the molecular (x, y, z) and lab (X, Y, Z) coordinate systems are shown in Figure 1. MD simulations of a monolayer of R-BN on water

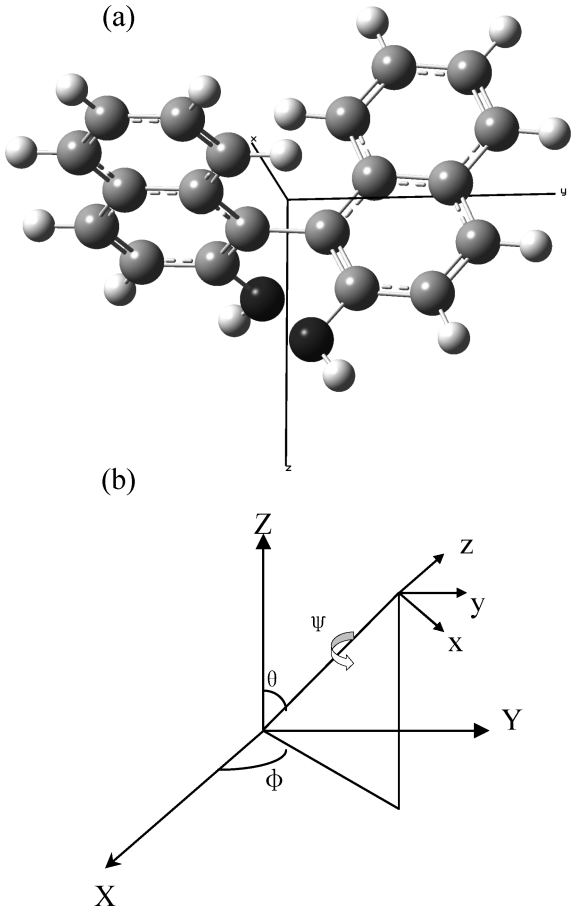

Figure 1. (a) Molecular structure of R-BN; (b) Euler angles relating the molecular (x,y,z) and lab coordinate (X,Y,Z) systems.

surface are performed with the generalized Amber force field (GAFF) for R-BN and SPC-E force field for water at the temperature of 300 K using the Gromacs program.[30] The simulation system is built through the following procedure: A simulation box containing 3560 waters is first generated by Gromacs. The R-BN monolayer containing 50 R-BNs is then added on the top and bottom of water in Z direction, with hydroxides of R-BNs in contact with the water molecules. Afterward, the system is minimized and equilibrated for 2 ns in the NPT ensemble. The corresponding equilibrated simulation box sizes are 61.8, 51.5, and 45.4 along X, Y, and Z direction, respectively. We then add a proper vacuum volume by changing the Z direction to 99.0 Å to generate the R-BN monolayer on water surface. Subsequently, NVT simulation with 100 ns is performed to generate the trajectory for further analysis. The long-range electrostatic interactions are treated by the particle-mesh Ewald (PME) summation.[31,32] Periodic boundary condition (PBC) is applied in all simulations. Bond lengths of all bonds with H-atoms are constrained using the LINCS algorithm.[33] A time step of 2 fs is used.

The normalized distributions of the three Euler angles θ, ψ, and ϕ are plotted in Figure 2. We can see from Figure 2a that

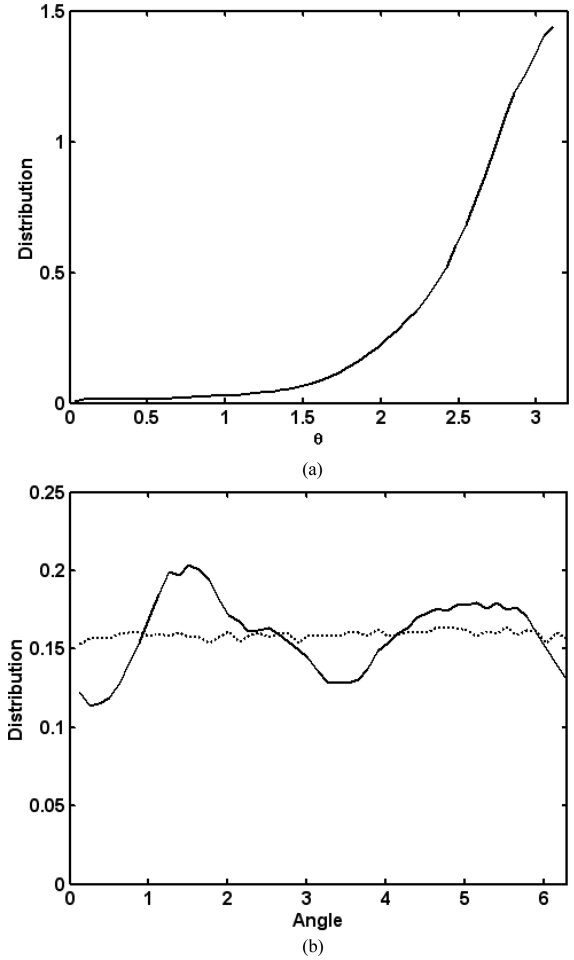

Figure 2. (a) θ-, (b) ψ- (solid line), and ϕ-dependent (dotted line) distributions of a monolayer of R-BN molecules on the water surface.

the distribution of θ is peaked at 180°, indicating that most of R-BN molecules form hydrogen bonds with water molecules and the most probable tilt angles are about 0°. The θ-dependent distribution also has a Gaussian shape, with a half width at half-maximum of 30°. The relation between the surface SFVS and the distribution can be found in ref 26 and a simplified relation is presented in section 3.4. The ψ-dependent distribution is also not uniform, with two peaks at 86 and 280°, which are due to the two OH groups of R-BN. Note that in this paper and ref 26, the Euler angles are defined in the y-convention. In the x-convention, the two peaks are about 0 and 190° (close to 180°), which indicates that R-BN molecules prefer to stand on water surface in a standard orientation (see Figures 1a). The ϕ-dependent distribution is uniform, which agree with the result from the theoretical prediction and physical considerations.[26] Figure 1 shows that the distribution

dx.doi.org/10.1021/jp400818d | J. Phys. Chem. C 2013, 117, 11117−11123

Table 1. Vibrational Frequencies (cm^{-1}), IR Intensity (km/mol), and the Corresponding Displacements between the Ground and the First Excited Electronic States Calculated by Excited Forces, Calculated Relative Raman Intensity (arbitrary unit), Isotropic, Anisotropy, and Antisymmetric Placzek Invariants Σ^0, Σ^2, and Σ^1 (in the Unit of 10^{-80} ($C \cdot m^2/V)^2$), and the Depolarization Ratios ρ

frequency	IR intensity	displacement Δ_t	Raman intensity	Σ^0	Σ^1	Σ^2	ρ
1244.9 A	0.335	0.058	1.661	0.575	0.053	1.160	0.360
1264.8 B	114.258	0.000	1.987	0.000	2.640	0.530	6.982
1293.9 B	73.671	0.000	1.877	0.000	2.467	0.520	6.684
1295.6 A	114.983	−0.081	5.251	1.846	0.060	3.704	0.343
1314.2 A	71.639	−0.117	7.659	2.712	0.015	5.427	0.335
1366.6 B	81.786	0.000	1.145	0.000	1.466	0.345	6.057
1370.5 A	42.659	0.053	3.115	1.076	0.105	2.176	0.362
1392.5 B	1.500	0.000	4.853	0.000	6.155	1.504	5.867
1397.0 A	0.510	−0.523	100.0	35.457	0.015	70.916	0.334
1412.6 B	15.140	0.000	0.272	0.000	0.342	0.086	5.729
1430.0 A	0.003	0.070	2.495	0.885	0.001	1.769	0.334
1462.0 B	25.674	0.000	0.412	0.000	0.510	0.136	5.425
1464.6 A	17.331	0.104	7.102	2.512	0.024	5.030	0.336
1501.1 B	4.102	0.000	0.010	0.000	0.013	0.004	5.212
1508.9 A	11.058	−0.126	9.815	3.450	0.106	6.928	0.343
1543.4 B	48.691	0.000	0.545	0.000	0.657	0.193	5.007
1546.2 A	39.990	−0.017	0.932	0.307	0.082	0.637	0.413
1616.3 B	7.578	0.000	0.899	0.000	1.060	0.336	4.701
1621.7 A	10.094	−0.518	88.87	31.465	0.210	62.951	0.335
1642.1 B	14.544	0.000	0.919	0.000	1.076	0.349	4.605
1646.7 A	10.304	0.181	12.12	4.229	0.239	8.524	0.350
1659.8 B	42.756	0.000	7.254	0.000	8.449	2.784	4.543
1661.1 A	39.143	0.037	4.962	1.470	0.954	3.252	0.524

of the Euler angles is broad. The broad distribution of the orientation angles indicates that the BN molecule is weakly ordered. This is likely due to the fact that BN is a large molecule, and its interactions with the water molecules are relatively weak.

3.2. Quantum Chemistry Calculations. Using density functional theory B3LYP/6-311++G** with Gaussian 09,[34] we optimize the structure of the ground state for R-BN, and then calculate the vibrational frequencies, IR intensity (see Table 1), and Hessian matrix. By diagonalizing the Hessian matrix we obtain the transformation matrix between the Cartesian coordinates and the normal coordinates. By applying time-dependent density functional theory (TDDFT) with the B3LYP functional, we compute the excited state and the corresponding excited energies, electric transition dipole moments between the ground and excited electronic states, and oscillator strengths, which are presented in Table S1. The displacements of each normal mode are calculated using the method proposed by Silverstein and Jensen[35] and are listed in Table 1. This method uses the forces of the excited state at the equilibrium structure of the ground state to construct a displaced harmonic oscillator model, which is rather efficiently for relatively large molecules.

In order to know the Raman B term, we need to calculate the derivatives of electric transition dipole moments with respect to the normal coordinates. We first calculate such derivatives with respect to the Cartesian coordinates using numerical difference, and then obtain the dipole moment derivatives with respect to the normal coordinates.

In order to obtain the line width of the excited state, we have fit the absorption spectra of Figure 1 in ref 10 with three Gaussian functions and find that the corresponding fwhm line width is 1183 cm^{-1}, which is approximately taken to be 1200 cm^{-1}. Similarly, the IR line width is taken by fitting Figure 2 of ref 10. Although different vibrational modes may have different linewidths, they do not differ significantly. So all the IR linewidths are taken to be $\Gamma = 12$ cm^{-1} and the corresponding fwhm IR linewidths are 24 cm^{-1}. The Lorentz formula for local-field factors $l(\omega_i) = (\varepsilon(\omega_i) + 2)/3$, with $\varepsilon(\omega_i)$ being 1.46, 1.39, and 1.37 at ω_i, are equal to ω_s, ω_1, and ω_2, respectively.[36,37]

Within the Condon approximation and displaced harmonic oscillator model, the absorption spectra can be calculated analytically[38,39] (see e.g., eq (2.33) in ref 39). We compute the R-BN absorption spectra. The result indicates that that the second peak in the experimental absorption spectra is due to the Franck−Condon progression (see Figure S1) with vibrational displacements around 670−4000 cm^{-1}. The detailed discussion is presented in Supporting Information.

3.3. Resonance Raman. As we know, the SFVS intensity is related to both the Raman and IR process. Doubly resonant SFVS is related to resonance Raman. The experimental resonance Raman spectra can thus provide important validation of the calculated normal mode displacements. Hence, in the subsection, we study resonance Raman of R-BN in the range of 1250−1700 cm^{-1} based on the theoretical potential energy shifts. In ref 40, Li et al. have studied UV near-resonance Raman spectroscopy of BN solutions in a 3 M NaOH aqueous solution with an excited light of frequency 325 nm. In NaOH solution, there is BN dianion (BN^{2-}), which avoids aggregation of the BN molecules.[40] Nevertheless, we can assume that the C═C stretching motion in the 1250−1700 cm^{-1} region are not significantly affected.

In Figure 3, we plot resonance Raman spectra for R-BN molecules at a frequency of 0.03 eV larger than the calculated first excited state. The corresponding Raman intensity, isotropic, anisotropy, antisymmetric Placzek invariants, and

dx.doi.org/10.1021/jp400818d | J. Phys. Chem. C 2013, 117, 11117−11123

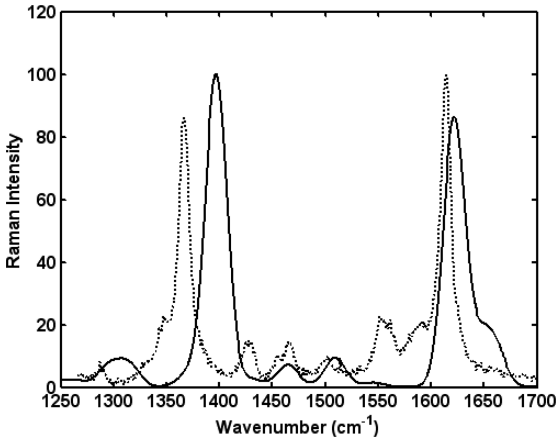

Figure 3. Calculated resonance Raman spectroscopy for R-BN molecules with excitation light 0.03 eV larger than the calculated first excited state energy (solid line) and experimental resonance Raman spectrum of BN in a 3 M NaOH aqueous solution with excitation frequency of 325 nm from ref 38 (dotted line).

the depolarization ratios are listed in Table 1. Equations to calculate the Placzek invariants and Raman spectra can be found in ref 41. The 1397.0 and 1621.7 A modes with large displacements are the two most intense modes. This agrees with the experiment[40] where the two most intense modes of BN^{2-} are 1366 and 1612 cm^{-1}. The depolarization ratios of the 1366 and 1612 cm^{-1} bands in experimental resonance Raman spectra of BN^{2-} at 325 nm are measured as 0.42 and 0.47, the calculated values of 1397.0 and 1621.7 A modes are 0.333 and 0.335. This difference between theoretical and experimental depolarization ratios may have been caused by an overestimation of the displacements and underestimation of the derivatives of electric dipole transition moments in the theoretical calculation.

The large displacements of the 1397.0 and 1621.7 A modes (−0.523 and −0.518, respectively) are the reason that they are the two most intense Raman modes. However, the IR intensity of the 1397.0 A mode is rather small with the value of 0.509 km/mol and that of 1621.7 A mode is 10.093 km/mol. Because only the modes with both large IR and Raman intensity can give strong SFVS signal, the SFVS of the 1397.0 A mode is very weak and that of 1621.7 A mode is stronger.

An interesting finding in Table 1 is that all the non-totally symmetric vibrational modes have abnormal depolarization ratios, which are larger than 0.75. In the nonresonant case, for a non-totally symmetric mode, there is no antisymmetric Raman polarizability and its depolarization ratio is always smaller than 0.75.[41] In the resonant case, the Raman A term is symmetric and the Raman B term can be asymmetric. For a non-totally symmetric mode, the Raman A term is zero and the Raman B term dominates. Its isotropic Placzek invariant is zero, while its anisotropy and antisymmetric Placzek invariants can be of the same order of magnitude. Thus, it may lead to an abnormal depolarization ratio, as shown in Table 1. However, resonance Raman intensity from Raman B term is relatively weak, such that it may be hard to directly observe the abnormal depolarization ratios of BN.

3.4. Surface SFVS for R-BN. After obtaining the orientational distributions of the R-BN molecules on water surface, their IR intensities, the displacements between ground and excited potential energy surfaces, electric transition dipole moments, and their derivatives, we calculate the surface doubly resonant SFVS using eqs 2 and 4−7, and the result is shown in Figure 4. When we calculate the SFVS, the light frequency is

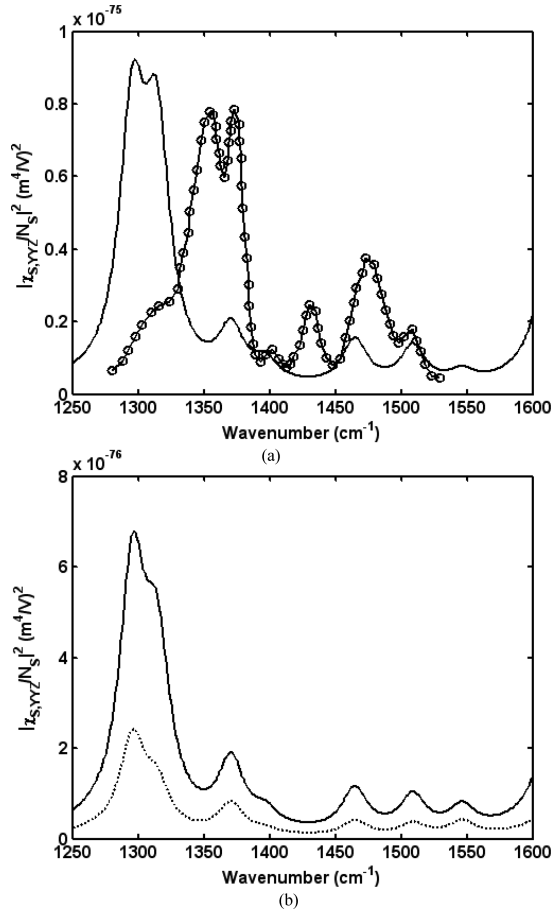

Figure 4. Surface SFVS of a monolayer of R-BN molecules on water at (a) 3.8622 eV (sum-frequency light 0.03 eV larger than the first excited state energy) and experimental surface SFVS (open circles) from ref 10, (b) 3.8122 eV (sum-frequency light 0.02 eV smaller than the first excited state energy, solid line) and 3.7522 eV (sum-frequency light 0.08 eV smaller than the first excited state energy, dotted line).

taken to be 0.03 eV larger than the excited energy of the first excited state, which is consistent with experiment.[10] In the calculation, only the first excited state is included. Because the calculated oscillator strength of the first excited is 0.0304, which is much larger than that of the second excited state, with a value of 0.0001. Such that the second excited state has little influence on the surface SFVS. The calculated most intense SFVS peak is about 9×10^{-76} $(m^4/V)^2$ and the experimental one is 8×10^{-76} $(m^4/V)^2$. The theoretical value is in good agreement to experiment. In the resonant case, the intense SFVS peaks are from the vibrational modes with both strong IR intensities and large displacements. The difference between the calculated frequencies and experimental ones should be due to the inaccuracy of Hessian matrix from quantum chemistry calculations.

In order to study the dependence of the surface SFVS on the UV frequency, in Figure 4b we also plot the SFVS when the relative sum-frequencies to the first absorption peak are at −0.02 and −0.08 eV, respectively. So, in the resonant case, SFVS is very sensitive to the UV frequency.

In Figure 5 we present surface SFVS from the contributions of Raman A and B terms, respectively. Figure 5 shows that

dx.doi.org/10.1021/jp400818d | J. Phys. Chem. C 2013, 117, 11117−11123

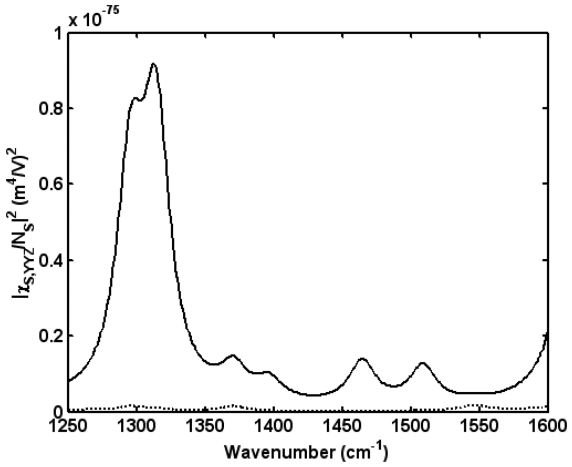

Figure 5. Surface SFVS of a monolayer of R-BN molecules on water contributions from Raman A term (solid line) and Raman B term (dotted line) at 3.8622 eV (sum-frequency light 0.03 eV larger than the first excited state energy).

surface SFVS are mainly from the Raman A term. The magnitude of contribution of Raman B term can be of the order of 10^{-77} $(m^4/V)^2$, which is at least 1 order of magnitude smaller than that from Raman A term. By comparing Figure 5 with Figure 4, we find that the SFVS intensity of the 1314.2 A mode become slightly weaker when including Raman B term.

In Figure 6, we plot the SFVS intensity dependence of the 1314.2 A mode on the orientating angles θ and ψ. From this

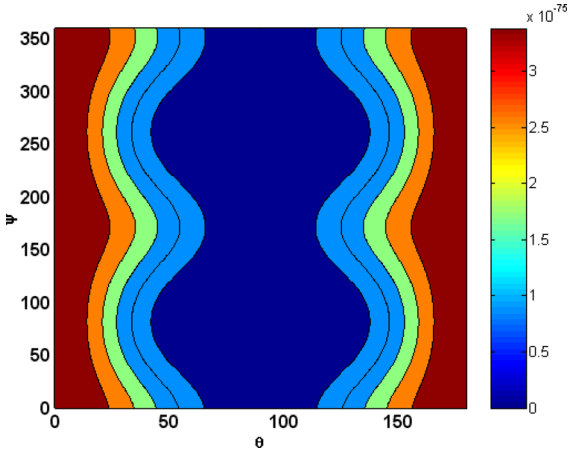

Figure 6. SFVS intensity dependence of the 1314.2 A mode on the Euler angles θ and ψ.

figure, we find that when θ is close to 0 or 180°, the SFVS intensity becomes most intense. We will show that the SFVS intensity distribution can be explained using the following eq 8.

The 1314.2 A mode gives the strongest peak in the SFVS experiment. We then further analyze the origin of the SFVS signal, and the properties of the hyperpolarizabity tensor associated with this peak. It is a totally symmetric mode with IR intensity of 71.6 km/mol, and its displacement is −0.117. The *x*, *y*, and *z* components of IR electric dipole derivatives of the 1314.2 A mode are 0.000, 0.000, and −0.2710 au, respectively, in the standard orientation shown in Figure 1. For the totally symmetric mode of R-BN with C_2 symmetry, the IR electric dipole derivative is also along the *z* direction in the standard orientation. The first excited state of BN is of B symmetry and its electric transition dipole moments are along the *x* and *y* directions with the values of 0.0772 and −0.5640 au, respectively. Since the *y* component is about 1 order of magnitude larger than the *x* component, when only the Raman A term is considered, the largest SFVS hyperpolarizability is the *yyz* component with a value of $(-7.4 + 5.9i) \times 10^{-38}$ m^4/V. Hence, the surface nonlinear susceptibility $\chi_S^{(2)}$ is approximately proportional to[26]

$$\chi_{YYZ}^{(2)} \propto \alpha_{yyz}^{(2)} \cos\theta - \alpha_{yyz}^{(2)} \sin^2\theta \cos\theta \sin^2\psi \quad (8)$$

Equation 8 is a result of the isotropic average of in-plane rotation angle, and it explains the results presented in Figure 6. When calculating the SFVS signal, it needs to be averaged over θ and ψ to obtain the surface susceptibility. The average $\langle \sin^2\theta \cos\theta \sin^2\psi \rangle$ is smaller than $\langle \cos\theta \rangle$, and the dominant term is $\langle \cos\theta \rangle \alpha_{yyz}^{(2)}$. Similar analysis can be performed for all the totally symmetric modes. We can see that although the relation between the surface nonlinear susceptibility and molecular hyperpolarizability is mathematically rather complex, a simple understanding of it can be obtained using molecular symmetry analysis and theoretical calculations.

From Table 1, we see that the displacement is zero when the vibrational mode is of B symmetry, which do not contribute to surface SFVS from Raman A term. For the B mode, the *x* and *y* components of IR electric dipole derivative are nonzero, and the *z* component of the electric transition dipole moment derivative is nonzero. Thus, the corresponding large nonzero hyperpolarizability components are *zyx*, *yzx*, *zyy*, and *yzy*. These peaks from the Raman B term are much smaller, and their symmetry properties can in principle be analyzed in a similar way as the totally symmetric modes, which will not be discussed further in this work.

4. CONCLUSIONS

In this work, we study a monolayer of R-BN molecules on water surface with a combination of theoretical methods. Molecular dynamics simulations show that the tilt angle distribution is of Gaussian type with the center around 180°, which indicates that R-BN molecules prefer to stand vertically on the surface by forming two hydrogen bonds with the water molecules. With DFT, we compute the ground state and IR intensity, and with TDDFT, we obtain the forces of the excited state. Then we calculate the displacements of potential energy surfaces along the normal coordinate between the ground and excited states. Derivatives of electric transition dipole moments are calculated using numerical difference. By combining the above results, we calculate the surface doubly resonant SFVS for R-BN monolayer on water surfaces. The calculated doubly resonant SFVS agrees well with experiment.

We then analyze the origins of the SFVS spectra and symmetric properties of the hyperpolarizability tensor associated with the 1314.2 cm^{-1} peak. For the R-BN molecule, the number of nonzero SFVS components can be significantly reduced by symmetry considerations that, in turn, can simplify the analysis of the experimental spectra.

The surface hyperpolarizability tensor is important in analyzing the SFVS spectra to obtain the molecular orientations on the surface. For molecules without symmetry, all three IR components and nine Raman components may exist, resulting in many possible terms. It is, thus, very hard to obtain them directly through experiments. The sum-over-states calculation schemes presented in this study can be used to obtain the SFVS

surface hyperpolarizability and help to identify the most important components, which are certainly helpful for SFVS experimental analysis in such cases.

■ ASSOCIATED CONTENT

Supporting Information

Absorption spectra calculation, excited state energies, electric transition dipole moments, and oscillator strength for R-BN molecule. This material is available free of charge via the Internet at http://pubs.acs.org.

■ AUTHOR INFORMATION

Corresponding Author

*E-mail: zrh@iccas.ac.cn (R.-h.Z.); qshi@iccas.ac.cn (Q.S.).

Notes

The authors declare no competing financial interest.

■ ACKNOWLEDGMENTS

This work is supported by National Natural Science Foundation (NNSF) of China (20903101, 91027015, 21103003, 21290194), the 973 Program (Grant No. 2011CB808502), and the Chinese Academy of Sciences through the Hundred Talents Project.

■ REFERENCES

(1) McGuire, J. A.; Shen, Y. R. *Science* **2006**, *313*, 1945.
(2) Wang, H.-F.; Gan, W.; Lu, R.; Rao, Y.; Wu, B.-H. *Int. Rev. Phys. Chem.* **2005**, *24*, 191.
(3) Richmond, G. L. *Chem. Rev.* **2002**, *102*, 2693.
(4) Eisenthal, K. B. *Chem. Rev.* **1996**, *96*, 1343.
(5) Chen, Z.; Shen, Y. R.; Somorjai, G. A. *Annu. Rev. Phys. Chem.* **2002**, *53*, 437.
(6) Xiong, W.; Laaser, J. E.; Mehlenbacher, R. D.; Zanni, Martin. T. *Proc. Natl. Acad. Sci. U.S.A.* **2011**, *108*, 20902.
(7) Stiopkin, I. V.; Weeraman, C.; Pieniazek, P. A.; Shalhout, F. Y.; Skinner, J. L.; Benderskii, A. V. *Nature* **2011**, *474*, 192.
(8) Carter, J. A.; Wang, Z. H.; Dlott, D. D. *Acc. Chem. Res.* **2009**, *42*, 1343.
(9) Simpson, G. J.; Rowlen, K. L. *Acc. Chem. Res.* **2000**, *33*, 781.
(10) Belkin, M. A.; Shen, Y. R. *Phys. Rev. Lett.* **2003**, *91*, 213907.
(11) Belkin, M. A.; Kulakov, T. A.; Ernst, K. H.; Yan, L.; Shen, Y. R. *Phys. Rev. Lett.* **2000**, *85*, 4474.
(12) Belkin, M. A.; Han, S.-H.; Wei, X.; Shen, Y. R. *Phys. Rev. Lett.* **2001**, *87*, 113001.
(13) Fischer, P.; Wiersma, D. S.; Righini, R.; Champagne, B.; Buckingham, A. D. *Phys. Rev. Lett.* **2000**, *85*, 4253.
(14) Raschke, M. B.; Hayashi, M.; Lin, S. H.; Shen, Y. R. *Chem. Phys. Lett.* **2002**, *359*, 367.
(15) Chen, X.; Tang, H.; Even, M. A.; Wang, J.; Tew, G. N.; Chen, Z. *J. Am. Chem. Soc.* **2006**, *128*, 2711.
(16) Ehland, F.; Hassing, S.; Dreybrodt, W. *J. Raman Spectrosc.* **1999**, *30*, 573.
(17) Benjamin, I. *Phys. Rev. Lett.* **1994**, *73*, 2083.
(18) Yeh, Y. L.; Zhang, C.; Held, H.; Mebel, A. M.; Wei, X.; Lin, S. H.; Shen, Y. R. *J. Chem. Phys.* **2001**, *114*, 1837.
(19) Morita, A.; Hynes, J. T. *Chem. Phys.* **2000**, *258*, 371.
(20) Morita, A.; Hynes, J. T. *J. Phys. Chem. B* **2002**, *106*, 673.
(21) Brown, M. G.; Walker, D. S.; Raymond, E. A.; Richmond, G. L. *J. Phys. Chem. B* **2003**, *107*, 237.
(22) Perry, A.; Ahlborn, H.; Space, B.; Moore, P. B. *J. Chem. Phys.* **2003**, *118*, 8411.
(23) Feibelman, P. J. *Chem. Phys. Lett.* **2004**, *389*, 92.
(24) Morita, A. *Chem. Phys. Lett.* **2004**, *398*, 361.
(25) Buch, V. *J. Phys. Chem. B* **2005**, *109*, 17771.
(26) Moad, A. J.; Simpson, G. J. *J. Phys. Chem. B* **2004**, *108*, 3548.
(27) Warshel, A.; Dauber, P. *J. Chem. Phys.* **1977**, *66*, 5477.
(28) Warshel, A. *Annu. Rev. Biophys. Bioeng.* **1977**, *6*, 273.
(29) Zheng, R.-H.; Chen, D.-M.; Wei, W.-M.; He, T.-J.; Liu, F.-C. *J. Phys. Chem. B* **2006**, *110*, 4480.
(30) van der Spoel, D.; Lindahl, E.; Hess, B.; van Buuren, A. R.; Apol, E.; Meulenhoff, P. J.; Tieleman, D. P.; Sijbers, A. L. T. M.; Feenstra, K. A.; van Drunen, R.; Berendsen, H. J. C. Gromacs User Manual, version 4.5; 2010, www.gromacs.org.
(31) Darden, T.; York, D.; Pedersen, L. *J. Chem. Phys.* **1993**, *98*, 10089.
(32) Essmann, U.; Perera, L.; Berkowitz, M. L.; Darden, T.; Lee, H.; Pedersen, L. G. *J. Chem. Phys.* **1995**, *103*, 8577.
(33) Hess, B.; Bekker, H.; Berendsen, H. J. C.; Fraaije, J. G. E. M. *J. Comput. Chem.* **1997**, *18*, 1463.
(34) Frisch, M. J. et al. *Gaussian 09*, Revision A.02; Gaussian, Inc.: Wallingford, CT, 2009.
(35) Silverstein, D. W.; Jensen, L. *J. Chem. Phys.* **2012**, *136*, 064111.
(36) Belkin, M. A.; Shen, Y. R. *Int. Rev. Phys. Chem.* **2005**, *24*, 257.
(37) Byers, J. D.; Hicks, J. M. *Chem. Phys. Lett.* **1994**, *231*, 216.
(38) Mukamel, S. *Principles of Nonlinear Optical Spectroscopy*; Oxford University Press: Oxford, 1995.
(39) Lin, S. H.; Chang, C. H.; Liang, K. K.; Chang, R.; Shiu, Y. J.; Zhang, J. M.; Hayashi, M.; Hsu, F. C. *Adv. Chem. Phys.* **2002**, *121*, 1.
(40) Li, Z.-Y.; Chen, D.-M.; He, T.-J.; Liu, F.-C. *J. Phys. Chem. A* **2007**, *111*, 4767.
(41) Mortensen, O. S.; Hassing, S. *Adv. Infrared Raman Spectrosc.* **1980**, *6*, 1.